PAPER

Improved understanding of the ball-pen probe through particle-in-cell simulations

IOP Publishing Plasma Physics and Controlled Fusion
Plasma Phys. Control. Fusion **59** (2017) 055007 (7pp) https://doi.org/10.1088/1361-6587/aa60d0

Improved understanding of the ball-pen probe through particle-in-cell simulations

S Murphy-Sugrue[1,2], J Harrison[1], N R Walkden[1], P Bryant[2] and J W Bradley[2]

[1] Culham Centre for Fusion Energy, Culham Science Centre, Abingdon, Oxon, OX14 3DB, United Kingdom
[2] Department of Electrical Engineering and Electronics, University Of Liverpool, Brownlow Hill, Liverpool, L69 3GJ, United Kingdom

E-mail: Sugrue@liverpool.ac.uk

Received 30 November 2016, revised 12 February 2017
Accepted for publication 16 February 2017
Published 21 March 2017

Abstract

Ball-pen probes (BPP) have been deployed in the SOL of numerous tokamak experiments and low-temperature magnetised plasmas to make direct measurements of the plasma potential and electron temperature. Despite strong empirical evidence for the success of the BPP it lacks a theoretical underpinning of its collection mechanism. In this paper we investigate the capability of the probe to measure the plasma potential by means of particle-in-cell simulations. The BPP is found to float at a potential offset from the plasma potential by a factor $T_e \alpha_{BPP}$. By simulating BPPs and Langmuir probes, excellent agreement has been found between the measured electron temperature and the specified source temperature. The transport mechanism for both ions and electrons has been determined. $E \times B$ drifts are observed to drive electrons and ions down the tunnel. This mechanism is sensitive to the diameter of the probe.

Keywords: particle-in-cell, ball-pen probe, Langmuir probe, plasma potential, electron temperature

(Some figures may appear in colour only in the online journal)

1. Introduction

Measurements of the plasma potential (Φ) and its fluctuations are vital for modelling transport phenomena in the edge region of tokamaks [1]. Turbulent structures (blobs) in the scrape-off layer are electrostatic and are advected towards the first-wall by $E \times B$ drifts arising from plasma potential fluctuations across the blob cross-section [2]. The strength and spatial scale of these potential fluctuations can be predicted, however robust measurements of such fluctuations are lacking making it difficult to fully validate models of radial transport in the SOL [3]. The theory of Langmuir probes allows the value of the plasma potential to be determined from the current (I)–voltage (V) curve of a Langmuir probe. Assuming the probe operates in the thin sheath limit, a simple expression [4] relates the floating potential of the probe (V_{LP}) to the local plasma potential

$$V_{LP} = \Phi - T_e \ln(R), \tag{1}$$

where T_e is the electron temperature in eV and R the ratio of the electron saturation current (I_{sat}^-) divided by the ion saturation current (I_{sat}^+). The logarithm of R is often denoted as α such that

$$\alpha_{LP} = \ln(R) = \ln\left(\frac{I_{sat}^-}{I_{sat}^+}\right). \tag{2}$$

In principle it is possible to sweep the bias voltage applied to a Langmuir probe to derive V_{LP}, T_e and α_{LP}. The local plasma potential can then be obtained from equation (1). However, in practice, especially in fusion plasmas, it is not possible to measure R. In these plasmas, probes operate in a restricted region of the I–V curve from floating to ion saturation. This allows measurements of n_e and T_e to be made while avoiding damage to the probe and the problem of spuriously high T_e measurements [5–8].

Various advanced probe techniques have been developed that aim to measure the plasma potential directly without needing an electron temperature measurement. These include

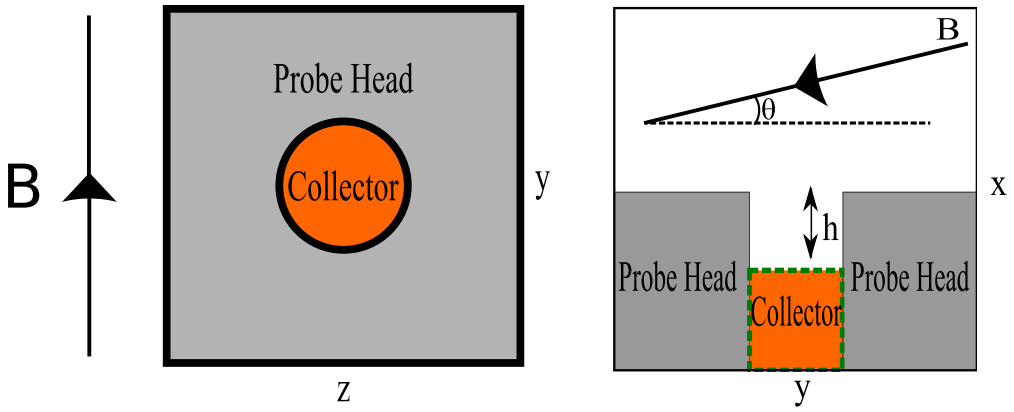

Figure 1. On the left—the BPP simulation domain as viewed from above looking along the x-axis. The collector sits at the bottom of the tunnel. On the right—a cross-section of the domain. h is the recession depth.

emissive probes [9] and the ball-pen probe (BPP) [10]. The emissive probe is not well suited to fusion plasmas as it requires a thin filament of wire to be exposed to the plasma making it structurally weak. Although this problem can be overcome with the use of laser heated emissive probes that do not require a thin filament of wire for operation and are therefore more robust [11]. The BPP is a robust diagnostic capable of surviving high heat loads [12]. The BPP was designed to reduce the ratio of saturation currents to unity so that the probe would float at the plasma potential as evident from equation (1). However, experiments find that $\alpha_{\mathrm{BPP}} = 0.6 \pm 0.3$ [13]. The BPP therefore gives a more direct estimate of the plasma potential than a conventional Langmuir probe but still requires a measurement of T_{e}. With a typical blob filament size on the order of a cm and velocities on the order of $\mathrm{km\,s^{-1}}$, microsecond time resolution is required to track the evolution of the potential between and during filament events [14]. The capability of the BPP to measure the plasma potential using a DC, floating measurement allows sufficient time resolution to measure these potential fluctuations [15].

The conventional BPP has a conical shaped collector, however, BPPs with flat collectors have been employed on MAST [12] and CASTOR [16]. The potential measurements from the CASTOR collectors were in good agreement with a conventional BPP. Despite empirical confirmation of the BPPs capabilities [1, 10, 17–19] the probe is lacking a model based on first principles to confirm the collection mechanism. In experiments, electron and ion currents reach the probe even when the collector is recessed beyond an ion Larmor radius. This was not predicted by the initial proposal for the collection mechanism [10].

Presented in this paper are the results of 3D particle-in-cell simulations of the flat BPP design, for a range of probe diameters and depths. The main aim of this study is to determine if the BPP is capable of measuring the plasma potential and gain insight into how particles travel down the tunnel, against the magnetic field, to the probe collector. The paper will also investigate the capability of the BPP, in conjunction with a floating Langmuir probe, to make electron temperature measurements. These simulations were carried out in three spatial and three velocity dimensions (3D3V), using VSim [20]. Collisions between ions and electrons are not included in these simulations and secondary electron emission is not considered. The simulation model is introduced in section 2 followed by a description of the transport mechanism in section 3. The capability of the probe to measure the plasma potential and electron temperature is explored in sections 4 and 5 respectively. The paper then moves on to explain the effects of probe diameter in section 6.1.

2. The simulation model

The simulation model is fully three dimensional (3D3V). The simulation domain captures a region of the probe head, the entire BPP tunnel down to the collector and a region of plasma above the probe at least four ion gyro-radii in depth in order to capture the magnetic presheath (MPS). The simulation domain is a cubic 3D Cartesian grid. The length of the domain varied for different probe diameters and depths. Lengths ranged between $3.5 \rightarrow 5$ mm for the x axis and $4.5 \rightarrow 5.5$ mm for the y and z axes. The collector lies in the y–z plane at the bottom of the probe tunnel as illustrated in figure 1. At the beginning of the simulation the plasma region is filled with a quasi-neutral plasma, with velocities sampled from a Maxwellian distribution. The motion of individual particles is tracked as they move due to self-consistent electric fields and an imposed uniform magnetic field. Particles that hit the probe structure deposit their charge to that location and are then deleted from the system. A charge density and electrostatic potential evolve naturally, to a steady state without imposing additional boundary conditions on the walls. Particles are injected along the top plane of the simulation at $x = 0$ to replenish those lost to the probe. The component of the velocity parallel to the magnetic field is sampled from the Emmert distribution [21]. The two perpendicular components are sampled from Maxwellian distributions. The y and z axis are periodic and the magnetic field makes an angle θ with the y-axis. The plasma potential is fixed at the top of the simulation to be 0 V.

Table 1. Typical plasma parameters used in the simulations of the BPP.

Magnetic field strength B	0.54 T
Magnetic field inclination θ	10°
Plasma density n	6.5×10^{17} m^{-3}
Electron temperature T_e	60 eV
Ion temperature T_i	60 eV
Ion Larmor radius ρ_i	1 mm
Electron mass m_e	9.11×10^{-31} kg
Ion mass m_i	900 m_e
Ion charge Z	1.6×10^{-19} C

The plasma density and temperature, modelled in the simulations was restricted by computational demands. Typical simulated parameters are shown in table 1. These values are close to those found in the SOL of MAST [22], however the simulated density is an order of magnitude lower than in experiments. Each grid cell in the PIC simulation was half a Debye length to prevent unphysical plasma heating in the simulations [23]. Increasing the density reduces the required grid spacing and so more grid cells are needed to simulate the same spatial region. To determine the effect of density, a selection of comparison simulations were carried out with an increased density of $n = 1.0 \times 10^{18}$ m^{-3} which is more in line with MAST's conditions. The increased density had no significant effect on the simulation results and so lower density simulations were run to produce the results presented in this paper.

BPPs in experiments are typically aligned such that the axis of the probe tunnel is perpendicular to the magnetic field, however, perfect alignment is rarely achieved. In these simulations, an angle θ was introduced as this was necessary for the particle injection algorithm. The source function and rate of injection required for perpendicular particle injection is not known. Simulations were carried out to determine the impact of θ. In these simulations θ was varied from $5° \rightarrow 15°$. Varying θ had no significant effect on the simulation results. The results presented in this paper are for a value of $\theta = 10°$. This value was chosen as it reduces the time it takes for the simulation to reach a steady state compared to the 5° case.

Collisions between charged particles are neglected in these simulations. The mean-free path (λ) for both electrons and ions significantly exceeds the length of the simulation domain (≈5 mm) for the plasma parameters used. From [24], using the stated simulated plasma parameters in table 1, $\lambda_{electron} = 7.2$ cm and $\lambda_{ion} = 10$ cm. As a result, particles can travel across the simulation domain multiple times without experiencing a collision. The simulation plasma consists of electrons and singly charged ions with no neutrals or impurities present. Charge exchange collisions between ions and neutrals are therefore neglected. Taking typical values for the MAST SOL, the neutral species present is deuterium with a density of $n = 1.0 \times 10^{19}$ m^{-3} and energy of 2.2 eV. Under these conditions the mean-free path for charge exchange interactions between the neutral atoms and the 60 eV ions is calculated to be 23.1 mm using reaction rates provided by Stangeby [25]. The ions are therefore able to traverse the simulation domain multiple times without experiencing a charge exchange collision. Plasma-surface interaction effects such as secondary electron emission and sputtering have also been neglected.

3. Transport mechanism

Electrons and ions are observed to reach the collector in both experiments [10] and the simulations even for collector recession depths beyond 2 ρ_i. This observation implies that a cross-field transport mechanism is present driving particles down the tunnel. In the bulk plasma, particles are born at the top of the domain and travel along field lines towards the probe where they will either encounter the top surface of the probe head or will enter the tunnel. From the viewpoint of an observer looking along magnetic field lines, the electron's clockwise orbit takes them towards the left hand side of the tunnel, while the anti-clockwise orbit of the ions takes them deep into the right hand side. This results in an electric field across the tunnel of the probe in the negative z direction. The potential structure within the probe tunnel and the resulting electric field is shown in figure 2.

The electric field in the z direction and magnetic field in the y direction results in an $E \times B$ drift that drives particles down the x-axis to the collector (for directions of coordinate axes the reader is referred to figure 1). Although the driving mechanism for the cross-field transport is the same for both species, their trajectories down the tunnel are very different. Once in the tunnel, particles will still continue to travel parallel to the field lines (along the y-axis) towards the tunnel wall. If a particle comes into contact with the tunnel wall it deposits its charge there and is lost from the simulation. In terms of motion parallel to the field, electrons are the more mobile species due to their low mass. As a result, a sheath forms in front of the floating tunnel wall to retard the flow of electrons. Only the most energetic electrons overcome this sheath potential to reach the wall. The less energetic electrons will reflect off the sheath and travel towards the other side of the tunnel. At the same time the electrons are driven down the tunnel due to the $E \times B$ drift. As a result, the electrons follow an oscillatory path down the tunnel. The trajectory of an electron, taken from the simulation, that reaches the collector is shown in figure 3.

The tunnel sheath acts to accelerate ions towards the wall so any ions that enter the sheath will be lost to the walls and unable to make it to the probe. Once entering the tunnel, an ion will continue its Larmor orbit while travelling parallel to the magnetic field towards the wall. To be collected an ion must have sufficient perpendicular velocity to make it to the probe before its parallel velocity takes it to the wall i.e.

$$\left(\frac{h}{v_\perp}\right) < \left(\frac{d}{v_\parallel}\right), \tag{3}$$

where h is the recession depth of the probe and d the tunnel diameter. Ions that reach the probe collector have a higher

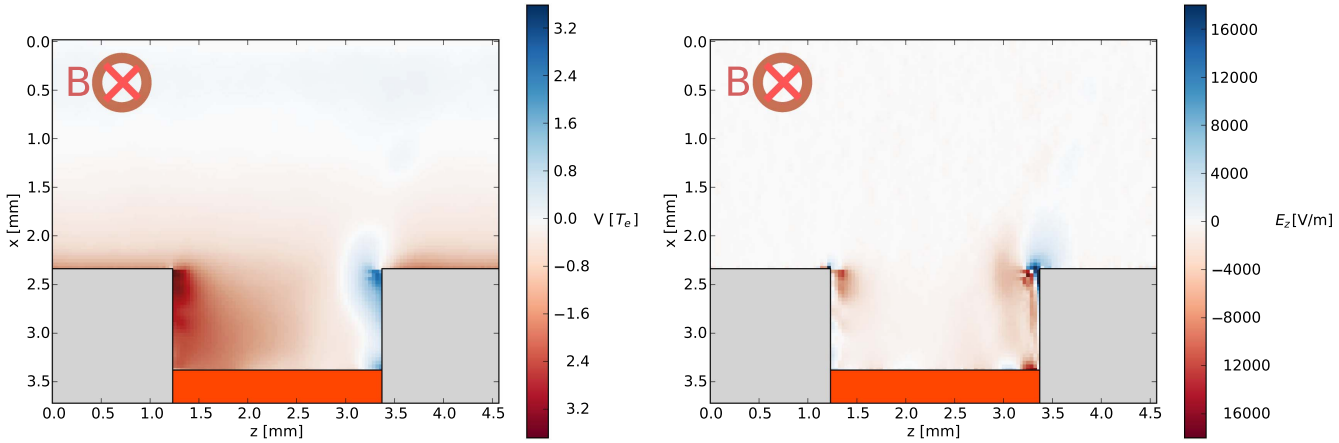

Figure 2. On the left—cross section of the electric potential. On the right—cross section of the resulting electric field in the z direction. Recession depth, $h = 1.1$ mm. Particles follow the magnetic field lines into and out of the plane shown. Their orbits can take them into contact with the walls, running parallel to the magnetic field, resulting in the potential structure shown.

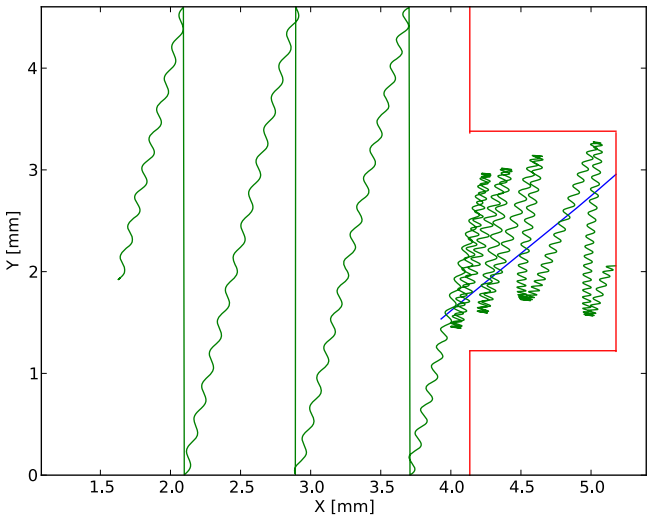

Figure 3. The trajectory of electrons and ions in the x–y plane is shown in green and blue respectively. Red lines show the walls of the probe. The electron follows the field across the periodic simulation domain until it enters the tunnel. Once in the tunnel the electron reflects back and forth due to the sheath potential. Vertical lines represent the electron leaving the simulation on one side of the periodic boundary and re-emerging on the other side. Ions simply travel down the tunnel due to their orbit while travelling parallel to the field. $h = 1.1$ mm.

perpendicular energy than parallel energy when they enter the tunnel. Their perpendicular speed is increased in the tunnel due to the $E \times B$ drift. The Larmor radius of the ion must also be sufficiently large so that the ion can reach the collector, i.e.

$$\rho_i \geqslant h. \tag{4}$$

The contract in the collection mechanism for ions and electrons was predicted in [18]. The collection mechanism suggests that the proportion of the electron population that can make it to the collector should not be sensitive to the probe tunnel diameter. The electron parallel velocity will always exceed the $E \times B$ drift velocity so electrons will encounter the wall sheath multiple times before they are able to drift to the collector. On the other hand, the collection of ions should be sensitive to the probe diameter. If the probe is too narrow, ions will not have time to complete enough of their orbit to make it to the collector before encountering the tunnel wall. The tunnel must be sufficiently wide so as not to hinder the collection of the ions. This is investigated in section 6.1.

4. Does the probe measure the plasma potential?

In order to test the capability of the BPP to measure the plasma potential, simulations were carried out for a probe of diameter 3.2 mm and a depth of 1.04 mm. A simulation was carried out with the probe operating in floating mode to obtain a floating potential measurement (V_{BPP}). Further simulations were carried out in order to determine R and α_{BPP}. In these simulations, the probe was biased positively and negatively with respect to the plasma potential in order to determine I_{sat}^{-} and I_{sat}^{+} respectively. It was observed that the currents for both species did not saturate. This behaviour has also been observed in experiments [26]. Following the method of [26], it was necessary to carry out further simulations with different probe bias voltages. The currents obtained at each voltage could then be extrapolated to obtain the value of R at the plasma potential.

The saturation currents increase linearly with probe bias, therefore it was possible to estimate R by linearly interpolating both currents to the plasma potential and defining their saturation values to be at this point. The values for the currents give $R = 3.02$ corresponding to a value $\alpha_{\mathrm{BPP}} = 1.1$. These values are higher than what is typically observed in experiments where α_{BPP} is in the range

$$\alpha_{\mathrm{BPP}} = 0.6 \pm 0.3. \tag{5}$$

However, these estimates were obtained using probes of at least 4 mm in diameter. In section 6.1, it is shown that a larger probe size reduces R closer to the value measured in experiments. Nevertheless, if it can be demonstrated that the BPP floats at a potential offset from the plasma potential by the

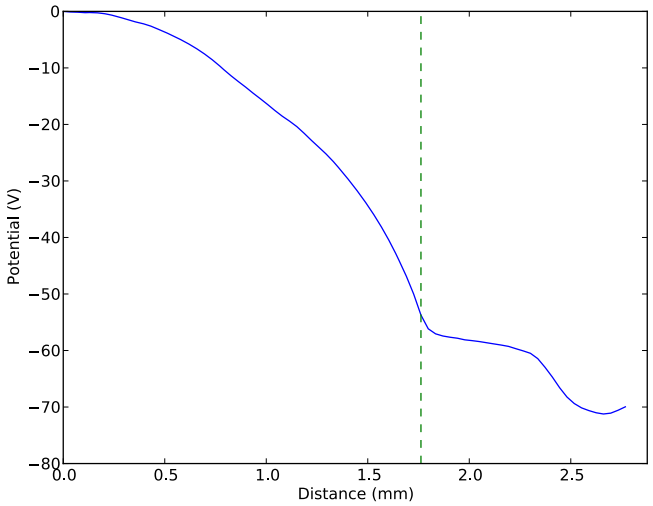

Figure 4. The plasma potential across the simulation domain, the dashed line shows the location of the BPP tunnel entrance.

product of $T_e\alpha_{BPP}$ then the BPP mechanism will be validated. Shown in figure 4 is a plot of the potential across the simulation domain along the x-axis. The potential at each point represents the average potential across a circular cross-section centred over the BPP collector. The plasma potential is defined as the value at the top of the domain, where the profile is flat before the MPS potential drop. The probe is found to float at a potential of -69 V relative to plasma potential. Based on the values of α_{BPP} and $T_e = 60$ eV, equation (1) predicts the plasma potential should be -3.8 V. This is very close to the value for the plasma potential in the simulation (0 V). The BPP will therefore float at a potential offset from the plasma potential by a factor of $T_e\alpha_{BPP}$. An $\alpha_{BPP} = 0$ would be required for the BPP to truly float at the plasma potential.

Simulations were carried out with an increased electron and ion temperature of 120 eV to determine if particle temperature had an impact on α_{BPP}. As before, multiple simulations were carried out for different probe bias voltages so that α_{BPP} could be measured by interpolating the currents. For these runs, a value of $\alpha_{BPP} = 1.38$ was observed, which is not significantly higher than the value found for $T_e = 60$ eV ($\alpha_{BPP} = 1.1$). It does not appear that the temperature strongly effects the operation of the BPP over the range of 60 eV $\leqslant T_e \leqslant$ 120 eV considered in this study.

5. Can the probe be used to make temperature measurements?

A combination of a BPP and a Langmuir probe can provide fast measurements of the electron temperature using a floating potential from each probe. By rearranging equation (1) for a Langmuir probe and a BPP we obtain

$$T_e = \frac{V_{BPP} - V_{LP}}{\alpha_{LP} - \alpha_{BPP}}. \tag{6}$$

This has yielded excellent agreement with Thomson scattering data on multiple tokamak experiments [18, 27]. For a planar Langmuir probe

$$\alpha_{LP} = -\frac{1}{2}\ln\left(2\pi\frac{m_e}{m_i}\left(1 + \frac{T_i}{T_e}\right)\right). \tag{7}$$

The BPP-LP method, using two DC measurements, then offers better time resolution compared to extracting T_e from the I–V curve of a Langmuir probe.

Additional simulations were carried out in order to test the capability of the BPP-LP pair to make electron temperature measurements. The BPP was replaced with a flush-mounted probe (FMP) and operated in floating mode to obtain V_{LP}. As discussed previously in section 4, α_{BPP} and V_{BPP} have already been measured. As in experiments, our simulations are not capable of measuring α_{LP}. In magnetised plasma the collection length of the probe operating in electron collection mode can extend very far into the plasma. It is not possible to capture this region in our simulation domain and so it is not possible to collect I^-_{sat}. Following experimental procedure we will therefore use the theoretical value for α_{LP} provided by equation (7).

As before, results are stated for the 3 mm diameter probe with an electron temperature of 60 eV. The FMP is found to float at a potential $V_{LP} = -129$ V. Combining this with $\alpha_{BPP} = 1.1$, $V_{BPP} = -69$ V and the theoretical value of $\alpha_{LP} = 2.14$ for the reduced ion mass we obtain a value of $T_e = 58.3$ eV which is in very good agreement with the specified temperature. This method is a viable way of making fast electron temperature measurements provided α_{BPP} is known. The measurement of T_e can be combined with V_{BPP} to determine the true plasma potential.

6. BPP design considerations

6.1. Effects of probe diameter

In order to investigate the effects of probe diameter, three probes of different width were simulated. The probe diameters were (a) 1.08 mm, (b) 2.16 mm and (c) 3.24 mm. All probes were recessed to the same depth of 1.04 mm. The ion Larmor radius in the simulations was $\rho_i = 1.02$ mm. For each probe diameter, three simulations were carried out: one with the probe operating in floating mode and two biased cases where the collector was in ion collection and electron collection mode. The floating potential of the collectors is shown in figure 5 along with the measured value of R. The ratios presented were obtained by dividing one current for each species. A linear interpolation has not been carried out so the true value of R is not known. The values are presented here as they demonstrate the effects of probe diameter on BPP measurements even if their absolute value is not correct.

With increasing width, a lower ratio R and a less negative value for V_{BPP} is observed. Beginning with the ions we find the current per unit area increases as the diameter increases. This is consistent with the collection mechanism: with a wider

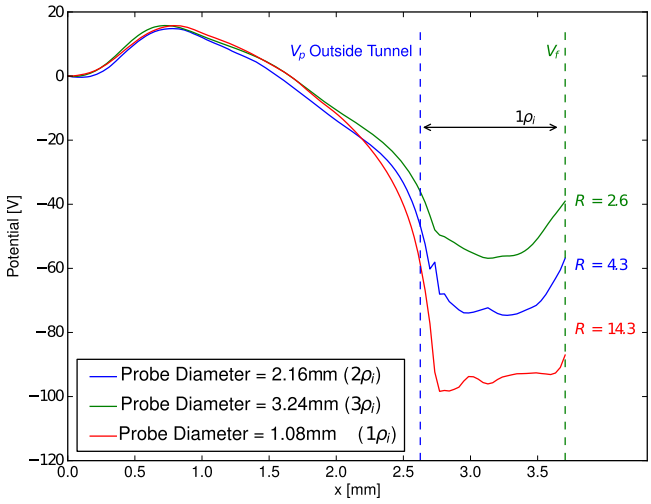

Figure 5. The potential structure across the simulation domain. The floating potential of the probe varies with tunnel diameter as does the value of R. The potential structure near $x = 0$ is a result of the source sheath, an artefact of particle injection in this region.

probe, ions have more time to reach the probe before their parallel motion brings them to a tunnel wall, therefore a higher proportion of the ion population reaches the probe. The electron current per unit area remains approximately constant with increasing probe diameter.

In order to allow a direct comparison with experiments, a set of simulations with a probe diameter of 4 mm and depth of 1 mm were carried out using a realistic ion mass and a field strength of 1.3 T, equivalent to the conditions used by Adámek *et al* in [10]. The following measurements were obtained.

$$R = 2.8 \quad \alpha_{\mathrm{BPP}} = 1.04 \quad V_{\mathrm{BPP}} = -67.6\ \mathrm{V} \tag{8}$$

which are in good agreement with equation (1). However, the value for α_{BPP} obtained in the simulations is outside the accepted range derived from experiments given in equation (5). This range is obtained using conical collectors where as the simulated probe was flat. The effects of BPP diameter were investigated on the linear plasma device Mirabelle [28]. However, due to the low magnetic field strength used in the experiments, the electron Larmor radius was comparable to the tunnel diameter. This regime of operation has not been considered in this paper. To the authors knowledge, an experimental comparison of the influence of probe diameter on the value R, for fusion relevant plasmas, has not been reported. However, in [16], three BPPs with a flat collector were placed into the edge region of CASTOR together with a BPP with a conical collector to make simultaneous measurements of the plasma potential. The flat collector probes were of different diameter: 1, 2 and 4 mm and the conical collector had a diameter of 2 mm. The authors concluded that the diameter was not a critical construction parameter but differences in the value of the measured plasma potential were observed. Values for R were not reported. Differences in the plasma potential measurements were attributed to a misalignment of the probes with the magnetic field. However, in the region of minimal curvature of the poloidal field, where the misalignment was lowest, it was found that the floating potential of the flat collector probes increased with probe diameter. If the floating potential of the probe varied with probe diameter, this could indicate that the value of R also changes with probe diameter. Out of the four probes, the 2 mm conical BPP was consistently found to float at the highest potential. This would suggest a smaller diameter conical BPP can achieve the same ratio R as a larger, flat collector BPP. The differences in potential measured in experiment were not as extreme as the differences found in the simulations. However, in the simulations, $T_{\mathrm{e}} = 60$ eV compared with $T_{\mathrm{e}} = 20$ eV in this experiment. This does not effect the capability of either probe to make plasma potential or electron temperature measurements, provided α_{BPP} is known for the probe that is employed.

6.2. Effect of probe recession

In the experiment described in [10] it was found that the value of R reached a minimum when the probe was recessed 0.5 mm ($1\rho_{\mathrm{i}}$). Once the probe was recessed beyond this depth, the value of R increased. Simulations have been carried out to test the sensitivity of R on collector recession and have found a similar trend. Both electron and ion currents to the probe decrease as the probe is recessed deeper into the tunnel, as more particles are absorbed by the tunnel walls. However, the electron current decreases less strongly than the ion current as electrons can reflect off the sheath formed along the interior walls of the probe while being driven towards the collector by $E \times B$ drifts. The reduced electron current is a result of the potential on the tunnel wall decreasing with depth into the tunnel, i.e. it becomes closer to the plasma potential. As a result, less of the electron population will be reflected by the weaker sheath potential. Increasing the probe depth makes it more likely that an ion's parallel velocity will take it into a tunnel wall before it can make it down to the collector. It appears that as long as the BPP is recessed beyond a few ρ_{e} the electrons become magnetically shielded and can only access the collector with $E \times B$ drifts. The probe then operates as a BPP. As long as this criteria is met and the probe depth is fixed with known α_{BPP} the probe depth is not thought to be an important parameter. However, beyond a certain depth, most ions will be absorbed before making it to the collector and the measurements will become dominated by noise. Simulations and experiments suggest a depth of 1 mm is sufficient for tokamak plasma conditions in order to reduce α_{BPP}.

7. Conclusions

3D3V PIC simulations have verified that the BPP measures a potential offset from the plasma potential by a factor $T_{\mathrm{e}}\alpha_{\mathrm{BPP}}$. BPPs in practice have obtained values as low as $\alpha_{\mathrm{BPP}} = 0.6$. For electron temperatures on the order of 10 eV, the difference between the floating potential of the BPP and the plasma potential will then be several volts. By simulating both an LP and a BPP the source temperature for the electrons was recovered, validating the BPP-LP method for making fast electron temperature measurements.

The mechanism that allows electrons to reach the collector even when it is recessed far beyond their Larmor radius

has been confirmed. Inside the tunnel, electrons oscillate along field lines, reflected by the wall sheaths, while simultaneously undergoing $E \times B$ drift motion towards the collector. This mechanism suggests probe diameter could be an important construction parameter. Further experimental measurements are needed to verify this. Probe depth is not an important consideration, provided the collector is recessed sufficiently such that the electrons are magnetically shielded from the collector. It was found that recessing the probe a depth greater than several ρ_e is sufficient. The voltage applied to a BPP should be swept initially in experiments to measure α_{BPP}. Once this value is acquired it is then possible to use the BPP to extract the electron temperature and plasma potential.

Acknowledgments

This project has received funding from the European Unions Horizon 2020 research and innovation programme under grant agreement number 633053 and from the RCUK Energy Programme [grant number EP/I501045]. To obtain further information on the data and models underlying this paper please contact PublicationsManager@ccfe.ac.uk*. The views and opinions expressed herein do not necessarily reflect those of the European Commission. This work made use of the facilities of N8 HPC Centre of Excellence, provided and funded by the N8 consortium and EPSRC (Grant No.EP/K000225/1). The Centre is co-ordinated by the Universities of Leeds and Manchester. This work was supported by the Engineering and Physical Sciences Research Council [EP/K504178/1].

References

[1] Adámek J, Rohde V, Müller H W, Herrmann A, Ionita C, Schrittwieser R, Mehlmann F, Stöckel J, Horacek J, Brotankova J and (ASDEX Upgrade Team) 2009 Direct measurements of the plasma potential in ELMy h-mode plasma with ball-pen probes on ASDEX upgrade tokamak *J. Nucl. Mater.* **390–391** 1114–7

[2] D'Ippolito D, Myra J and Zweben S 2011 Convective transport by intermittent blob-filaments: comparison of theory and experiment *Phys. Plasmas* **18** 060501

[3] Militello F, Tamain P, Fundamenski W, Kirk A, Naulin V, Nielsen A and (the MAST team) 2013 Experimental and numerical characterization of the turbulence in the scrape-off layer of mast *Plasma Phys. Control. Fusion* **55** 025005

[4] Stangeby P C and McCracken G M 1990 Plasma boundary phenomena in tokamaks *Nucl. Fusion* **30** 1225

[5] Tagle J, Stangeby P and Erents S 1987 Errors in measuring electron temperatures using a single langmuir probe in a magnetic field *Plasma Phys. Control. Fusion* **29** 297

[6] Matthews G 1994 Tokamak plasma diagnosis by electrical probes *Plasma Phys. Control. Fusion* **36** 1595

[7] Stangeby P 1995 Determination of T_e be in a magnetic field by directly measuring the probeas sheath drop using a pin-plate probe *Plasma Phys. Control. Fusion* **37** 1337

[8] Pitts R and Stangeby P 1990 Experimental tests of langmuir probe theory for strong magnetic fields *Plasma Phys. Control. Fusion* **32** 1237

[9] Schrittwieser R *et al* 2002 Measurements with an emissive probe in the castor tokamak *Plasma Phys. Control. Fusion* **44** 567

[10] Adámek J, Stöckel J, Hron M, Ryszawy J, Tichý M, Schrittwieser R, Ionită C, Balan P, Martines E and van Oost G 2004 A novel approach to direct measurement of the plasma potential *Czech. J. Phys.* **54** C95–9

[11] Schrittwieser R *et al* 2008 Laser-heated emissive plasma probe *Rev. Sci. Instrum.* **79** 083508

[12] Walkden N 2014 Properties of intermittent transport in the mega ampere spherical tokamak *PhD Thesis* University of York

[13] Silva C, Adámek J, Fernandes H and Figueiredo H 2015 Comparison of fluctuations properties measured by langmuir and ball-pen probes in the isttok boundary plasma *Plasma Phys. Control. Fusion* **57** 025003

[14] Boedo J *et al* 2014 Edge transport studies in the edge and scrape-off layer of the National Spherical Torus Experiment with Langmuir probes *Phys. of Plasmas* **21** 042309

[15] Horacek J *et al* 2010 Interpretation of fast measurements of plasma potential, temperature and density in SOL of ASDEX Upgrade *Nucl. Fusion* **50** 10

[16] Schrittwieser R, Ionita C, Adámek J, Stöckel J, Brotánková J, Martines E, Popa G, Costin C, van de Peppel L and van Oost G 2006 Direct measurements of the plasma potential by katsumata-type probes *Czech. J. Phys.* **56** B145–50

[17] Pánek R *et al* 2016 Status of the compass tokamak and characterization of the first h-mode *Plasma Phys. Control. Fusion* **58** 014015

[18] Walkden N R, Adámek J, Allan S, Dudson B D, Elmore S, Fishpool G, Harrison J, Kirk A and Komm M 2015 Profile measurements in the plasma edge of mega amp spherical tokamak using a ball pen probe *Rev. Sci. Instrum.* **86** 023510

[19] Adámek J, Peterka M, Gyergyek T, Kudrna P, Ramisch M, Stroth U, Cavalier J and Tichy M 2013 Application of the ball-pen probe in two low-temperature mag-netised plasma devices and in torsatron tj-k *Contrib. Plasma Phys.* **53** 39–44

[20] Nieter C and Cary J R 2004 Vorpal: a versatile plasma simulation code *J. Comput. Phys.* **196** 448–72

[21] Emmert G, Wieland R, Mense A and Davidson J 1980 Electric sheath and presheath in a collisionless, finite ion temperature plasma *Phys. Fluids* **23** 803–12

[22] Militello F, Fundamenski W, Naulin V and Nielsen A H 2012 Simulations of edge and scrape off layer turbulence in mega ampere spherical tokamak plasmas *Plasma Phys. Control. Fusion* **54** 095011

[23] Birdsall C and Langdon A 2005 *Plasma Physics via Computer Simulation* (*Series in Plasma Physics*) (New York: Taylor and Francis) Originally published: 1985, New York, London: McGraw-Hill

[24] Wesson J *et al* 1987 *Tokamaks* (New York, Oxford: Clarendon)

[25] Stangeby P C 2000 *The Plasma Boundary of Magnetic Fusion Devices* (*Plasma Physics Series*) (New York: Taylor and Francis)

[26] Adámek J *et al* (the COMPASS Team) 2017 Fast measurements of the electron temperature and parallel heat flux in elmy h-mode on the compass tokamak *Nucl. Fusion* **57** 022010

[27] Adámek J *et al* 2016 Profile measurements of the electron temperature on the asdex upgrade, compass, and isttok tokamak using thomson scattering, triple, and ball-pen probes *Rev. Sci. Instrum.* **87** 043510

[28] Bousselin G, Cavalier J, Pautex J F, Heuraux S, Lemoine N and Bonhomme G 2013 Design and validation of the ball-pen probe for measurements in a low-temperature magnetized plasma *Rev. Sci. Instrum.* **84** 013505